THE JOURNAL OF PHYSICAL CHEMISTRY C

Article

pubs.acs.org/JPCC

# Mn and Co Charge and Spin Evolutions in $LaMn_{1-x}Co_xO_3$ Nanoparticles

Mahnaz Ghiasi,*[†,‡] Mario Ulises Delgado-Jaime,[†] Azim Malekzadeh,[‡] Ru-Pan Wang,[†] Piter S. Miedema,[§] Martin Beye,[§] and Frank M. F. de Groot*[†]

[†]Inorganic Chemistry & Catalysis, Debye Institute for Nanomaterials Science, Utrecht University, Universiteitsweg 99, Utrecht 3584 CG, The Netherlands

[‡]School of Chemistry, Damghan University, 36715/364, Damghan, I. R. Iran

[§]Institute for Methods and Instrumentation for Synchrotron Radiation Research FG-ISRR, Helmholtz-Zentrum für Materialien und Energie GmbH, Albert-Einstein-Strasse 15, 12489 Berlin, Germany

Supporting Information

**ABSTRACT:** The charge and spin-state evolution of manganese and cobalt in the $LaMn_{1-x}Co_xO_3$ ($x$ = 0.00, 0.25, 0.50, 0.75, and 1.00) perovskite nanoparticles have been studied with soft X-ray absorption spectroscopy. The results show a gradual increase in the average oxidation state of both Mn and Co ions with cobalt doping. The average valence of the $LaMn_{1-x}Co_xO_3$ samples remains close to 3.0, with the Mn valence increasing from 3.1 to 4.0 and the Co valence increasing from 2.0 to 3.0. The symmetry of Mn and Co was determined using multiplet calculations. Calculating the intensity-area of the oxygen K pre-edge feature confirmed an increase in covalency with increasing Mn and Co oxidation state. The ground-state composition of $Mn^{3+}$ in $LaMnO_3$, and $Co^{3+}$ in $LaCoO_3$, was investigated, and it was found that $Mn^{3+}$ ($D_{4h}$) and $Co^{3+}$ ($O_h$) are mainly in their low-spin state, with 10−20% admixture of high-spin state contributions into a mixed spin ground state.

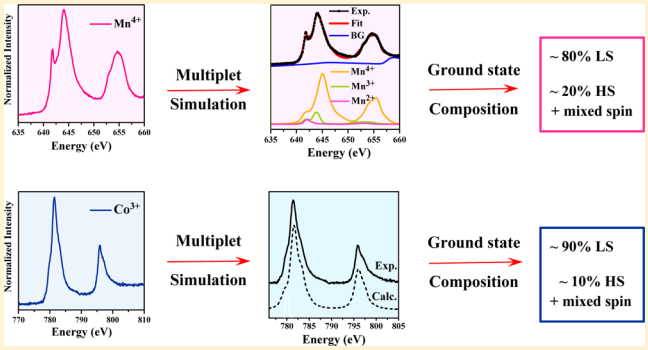


## 1. INTRODUCTION

Metal oxide perovskites have attracted large attention due to their wide range of functionality such as catalysis, superconductivity, gas sensors, and batteries.[1−3] Observation of giant magnetoresistance and colossal magnetoresistance (CMR) in manganites caused considerable interest in their potential applications, for example in spintronics.[4] The parent compound, $LaMnO_3$, is an insulator with orthorhombic perovskite structure which becomes antiferromagnetic below the Neel temperature ($T_N \approx 140$ K).[5] Occurrence of the mixed valence $Mn^{3+}/Mn^{4+}$ leads to the onset of the metallic ferromagnetic state. The mixed valence state can be created by changing the stoichiometric oxygen content or by partial substitution of lanthanum or manganese by divalent ions.[6,7]

A great deal of work has been performed regarding substitution of manganese with cobalt. Goodenough et al. concluded that the appearance of the ferromagnetism in the $LaMn_{1-x}Co_xO_3$ samples with $0 < x \leq 0.5$ is attributed to the superexchange interaction between $Mn^{3+}$ ions, without any magnetic contribution from low-spin $Co^{3+}$.[8] Later on, Park et al. mentioned the presence of CMR in $LaMn_{0.85}Co_{0.15}O_3$ and found out that the dopant Co is divalent where manganese becomes mixed valent.[9] They suggested that the ferromagnetic state observed in $LaMn_{1-x}Co_xO_3$ should be understood in the framework of a double-exchange mechanism of $Mn^{3+}/Mn^{4+}$. Despite not being consistent with the traditional idea about the ferromagnetic states in $LaMn_{1-x}Co_xO_3$ series, their findings provided a potential way for realizing CMR by Mn-site substitution. Further discussion is raised by the work of Troyanchuk and co-workers, who discussed the magnetic properties of $LaMn_{1-x}Co_xO_3$ in terms of the competition between positive $Mn^{3+}$−O−$Mn^{4+}$, $Mn^{3+}$−O−$Mn^{3+}$, $Co^{2+}$−O−$Mn^{4+}$ and negative $Mn^{4+}$−O−$Mn^{4+}$, $Co^{2+}$−O−$Co^{2+}$, $Mn^{3+}$−O−$Co^{2+}$ superexchange interactions.[10]

To resolve the Mn and Co local structure and valence states in $LaMn_{1-x}Co_xO_3$ perovskites, several X-ray absorption spectroscopy studies have been accomplished. For example, Sikora et al. studied the valence states of Mn and Co systematically by means of X-ray absorption spectroscopy (XAS) at the metal K-edges.[11] They suggested that at intermediate values of $x$, the transition metal ions are in their high spin states. In another study they observed a high spin state for $Mn^{3+}/Mn^{4+}$ and for $Co^{2+}$ in the entire range of $x$.[12] The $Co^{3+}$ revealed a low-spin state at low doping, while the average $Co^{3+}$ spin state showed an increase at

**Received:** January 28, 2016
**Revised:** March 25, 2016
**Published:** March 28, 2016





DOI: 10.1021/acs.jpcc.6b00949
J. Phys. Chem. C 2016, 120, 8167−8174

higher cobalt concentration. They claimed that this observation is due to a gradual charge transfer from Mn to Co sites upon increasing Co doping. Burnus et al. investigated $LaMn_{0.5}Co_{0.5}O_3$ by soft X-ray absorption spectroscopy and found a high-spin $Co^{2+}$−$Mn^{4+}$ valence state for this compound.[13] By means of soft X-ray magnetic circular dichroism spectroscopy (XMCD), they established that $Co^{2+}$ and $Mn^{4+}$ ions are ferromagnetically aligned. Using X-ray absorption fine structure (EXAFS) at K-edges, Palikundwar et al. pointed out that the local structure of $MnO_6$ octahedra is distorted and the distortion decreases with an increase in Co content. In contrast, the $CoO_6$ octahedra are undistorted over the entire composition range and have a single bond length for all six O atoms of the first coordination shell.[14]

Despite the extensive work that has been carried out on $LaMn_{1-x}Co_xO_3$ compounds to understand the effect of Co doping on lanthanum manganese perovskites, the detailed quantitative analysis still has to be improved. In this paper, we present a systematic XAS study to probe the valence states of manganese and cobalt in $LaMn_{1-x}Co_xO_3$ ($x$ = 0.00, 0.25, 0.50, 0.75, and 1.00) nanoperovskites. Moreover, the hybridization of the transition metals and oxygen states was investigated by O K-edge XAS to understand the electron sharing between O 2p and transition metal 3d states.

## 2. EXPERIMENTAL SECTION

The $LaMn_{1-x}Co_xO_3$ nanoperovskites were prepared by the citrate−nitrate autocombustion method using $La(NO_3)_3{\cdot}6H_2O$, $Co(NO_3)_2{\cdot}6H_2O$, and $Mn(NO_3)_2{\cdot}4H_2O$ precursors in the presence of citric acid as described previously.[3,15]

X-ray diffraction patterns of the freshly calcined samples were recorded in a Bruker AXS diffractometer D8 ADVANCE with Cu K$\alpha$ radiation filtered by a nickel monochromator and operated at 40 kV and 30 mA. Diffraction patterns were recorded in the range of $2\theta$ = 15−65° using a step size of 0.06.

The oxygen K-edge, Mn $L_{2,3}$ edge, and Co $L_{2,3}$ edge were collected at undulator Beamline UE52-SGM of the BESSY II synchrotron (Berlin). The measurements were collected in the total electron yield mode (by measuring the sample drain current) using the 1200 $mm^{-1}$ spherical grating of the UE52-SGM monochromator and the SolidFlexRIXS end-station. The pressure of the chamber was in the range of $9 \times 10^{-9}$ to $6 \times 10^{-8}$ mbar. All the spectra were collected at room temperature and normalized to the beam current, to correct for synchrotron-intensity loss during a measurement. To compare the spectra, they were normalized to 1.0 at the maximum peak.

## 3. COMPUTATIONAL SECTION

**3.1. Ligand Field Multiplet Calculations (LFM).** Co 2p XAS spectra were simulated using the Charge Transfer Multiplet for XAS program (CTM4XAS).[16] This program uses the multiplet model implemented by Thole,[17] based on the atomic theory developed by Cowan,[18] and the crystal field interactions described by Butler.[19] This approach includes both electron−electron interactions and spin−orbit coupling for each open subshell. Atomic Slater−Condon parameters ($F^{dd}$, $F^{pd}$, and $G^{pd}$) are scaled to 80% of the Hartree−Fock calculated values.[18] The Mn and Co $L_{2,3}$ spectra are calculated from the sum of all possible transitions for an electron excited from the 2p core level into an unoccupied 3d level. The ground state is approximated by the electronic configuration $3d^n$. In the ground state, 3d spin−orbit coupling and the crystal field affect the $3d^n$ configuration. The $3d^n$ ground state and the $2p^5 3d^{n+1}$ final state are affected by the 3d3d multiplet coupling. In the final state also the 2p3d multiplet coupling, the 2p and 3d spin−orbit couplings, and the crystal field potential in appropriate symmetry are included. The strength of the crystal field is described with empirical parameters 10 Dq, Ds, and Dt, and those are optimized to experiment.[20] To reduce bias, we tested a new methodology implemented in BlueprintXAS[21,22] to fit multiplet simulations to experiment by computing a large number of start points that span throughout the solution space to evaluate crystal field parameters and relative Mn compositions. In the present study, to generate the fit of $LaMnO_3$ and of $LaMn_{0.25}Co_{0.75}O_3$, 500 Monte Carlo starting points were used with a model that holistically included background and crystal field parameters for different Mn components.

**3.2. Fitting and Analysis of XAS spectra.** To quantify the relative amounts of $Co^{2+}/Co^{3+}$ and $Mn^{3+}/Mn^{4+}$ in the XAS spectra, a holistic model that included the background as well as normalized references for each component was developed to fit the Co and Mn L-edge XAS spectra. In this model, the normalized reference components were modeled in functional form such that the corresponding raw data is subject to background-subtraction and normalization, as part of the optimization procedure. Using Blueprint XAS, a family of good fits in each case was obtained.[21,22] From these fits the mixed valence composition of Co and Mn in each sample was evaluated.

In the case of the O K-edge, a model that included the pre-edge peaks, the background, the edge jump, and the La 5d character peaks was used to fit the experimental data, from which a family of fits was obtained. The data were then normalized with respect to the intensity area of the La 5d character band under the assumption that La covalency remains constant in $LaMn_{1-x}Co_xO_3$ series.

**3.3. Ground-State Symmetry Analysis.** To investigate the ground-state composition of $Mn^{3+}$ and $Co^{3+}$, the CTM4DOC program was used (unpublished results). This program projects the ground state into its individual components with respect to a specific interaction in terms of single-particle 3d orbitals.[23] This includes the projection to the combination of octahedral symmetry term symbols, atomic term symbols, and single-particle 3d orbitals.

## 4. RESULTS AND DISCUSSION

**4.1. XRD.** Shown in Figure 1 are the wide-angle XRD patterns of the $LaMn_{1-x}Co_xO_3$ perovskites. For analyzing the XRD data, a commercial Xpert package was used. Formation of a single perovskite phase is confirmed from the XRD profiles. The samples with $x$ < 0.5 show an orthorhombic structure belonging to space group *Pbnm* (X-pert high score PDF code: 01-088-0128). For the samples with $x$ > 0.5, a rhombohedral structure belonging to space group $R\bar{3}m$ (X-pert high score PDF code: 00-009-0358) is found. For the sample with 0.5 doping level, the diffractogram (Figure 1c) shows both the orthorhombic and rhombohedral structural phases. These results are consistent with the previous studies.[5,24] Analyzing the XRD data confirmed that the $LaMnO_3$, prepared in this study, has 3.3% excess oxygen, i.e., $LaMnO_{3.1}$, resulting in 20% $Mn^{4+}$. It was reported that the stoichiometric $LaMnO_3$ should be prepared in the absence of oxygen, and annealing in air results in the nonstoichiometric $LaMnO_{3+\delta}$.[25] The XRD data were used to calculate the crystallite size of perovskite phases using Scherrer and Williamson−Hall equations.[26] Detected phases are observed to be in the range of 30−40 nm.



DOI: 10.1021/acs.jpcc.6b00949
J. Phys. Chem. C 2016, 120, 8167−8174

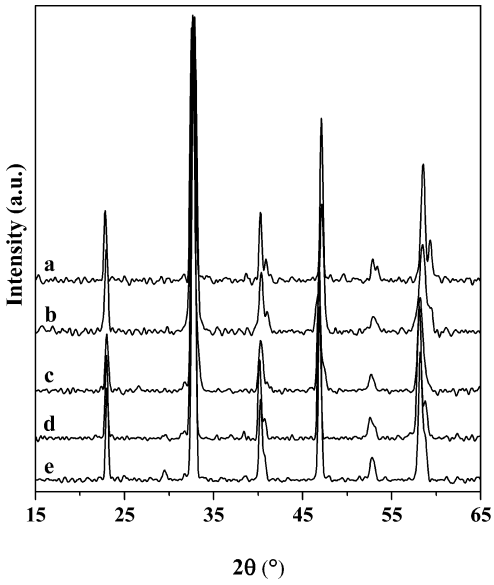


**Figure 1.** XRD patterns of (a) $LaCoO_3$, (b) $LaMn_{0.25}Co_{0.75}O_3$, (c) $LaMn_{0.5}Co_{0.5}O_3$, (d) $LaMn_{0.75}Co_{0.25}O_3$, and (e) $LaMnO_3$.

**4.2. Mn $L_{2,3}$ Edge.** The $L_{2,3}$ edge XAS spectra correspond to the transition to the outmost shell in 3d transition metal oxides, implying that the spectra are directly related to valence state changes. Figure 2 shows the normalized Mn $L_{2,3}$ absorption

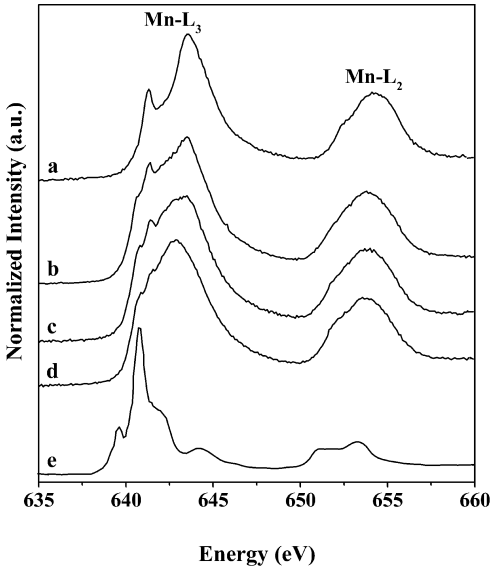


**Figure 2.** Mn $L_{2,3}$ XAS spectra of (a) $LaMn_{0.25}Co_{0.75}O_3$, (b) $LaMn_{0.5}Co_{0.5}O_3$, (c) $LaMn_{0.75}Co_{0.25}O_3$, (d) $LaMnO_3$, and (e) MnO. The MnO spectrum is reproduced from ref 28.

spectra of the samples together with MnO as the reference of $Mn^{2+}$. Results show a shift in the $L_3$ to higher energy from MnO to $LaMnO_3$. The shift to higher energies continues by doping the Mn by Co which reflects the increase of Mn valence state. It has been reported that upon oxidation from $Mn^{2+}$ to $Mn^{3+}$ and $Mn^{3+}$ to $Mn^{4+}$, the average shift in $L_3$ is on the order of 1.5−2 eV and 1−2 eV, respectively.[27] Comparing the spectra with previous reports demonstrates that the Mn species in $LaMnO_3$ and $LaMn_{0.25}Co_{0.75}O_3$ are $Mn^{3+}$ and $Mn^{4+}$, respectively.[13,27] It can be concluded that the Mn contained in the $LaMn_{0.75}Co_{0.25}O_3$ and $LaMn_{0.5}Co_{0.5}O_3$ consists of a mixture of $Mn^{3+}$and $Mn^{4+}$. By comparing the spectra with the MnO, as the reference of $Mn^{2+}$, it can be found that there is possibly some minor admixture of $Mn^{2+}$ in the samples.

To obtain multiplet simulation parameters and compositions most consistent to experimental data of $LaMnO_3$ and $LaMn_{0.25}Co_{0.75}O_3$, Blueprint XAS was used (Figure 3). The obtained fits reproduced well the experimental spectra, from which corresponding crystal field parameters are listed in Table 1. The 10 Dq values reported in Table 1 are the ground-state values. These results show that the Mn content of $LaMnO_3$ is not pure $Mn^{3+}$ and is an admixture of $Mn^{2+}$ (0.5%), $Mn^{3+}$ (59.4%), and $Mn^{4+}$ (40.1%), while the Mn content of $LaMn_{0.25}Co_{0.75}O_3$ is made of $Mn^{2+}$ (1.4%), $Mn^{3+}$ (8.5%), and $Mn^{4+}$ (90.1%). The $Mn^{3+}$ and $Mn^{4+}$ symmetry is considered to be $D_{4h}$ (due to a Jahn−Teller distortion) and $O_h$, respectively. Within this approach, charge transfer parameters were not considered. However, hybridization of the Mn and Co with oxygen, ligand atoms, is not negligible. This effect was included in the multiplet calculations by a reduction of the Slater integrals from their atomic values to account for isotropic covalency via a nephelauxetic effect.[29] The scaling factors (%) that were obtained from the fits to account for covalency were, of 52% ($F^{dd}$ and $F^{pd}$) for $Mn^{3+}$ in $LaMnO_3$ and of 50% ($F^{dd}$) and 42% ($F^{pd}$) for $Mn^{4+}$ in $LaMn_{0.25}Co_{0.75}O_3$;, confirming the covalent character of the Mn−O bonding.

These results on the Mn $L_{2,3}$ spectra for $LaMnO_3$ and $LaMn_{0.25}Co_{0.75}O_3$ suggest that the $Mn^{4+}/Mn^{3+}$ ratio is increasing with Co doping. A similar result was obtained by the work of Palikundwar and co-workers.[14] There are two possible explanations for the appearance of $Mn^{4+}$. One can be the presence of overstoichiometric oxygen, and the other is a $Mn^{3+} + Co^{3+} \rightarrow Mn^{4+} + Co^{2+}$ type of charge redistribution. To clarify the cause of the presence of $Mn^{3+}/Mn^{4+}$ mixture, the valence of the dopant Co in the manganese perovskites was also investigated by means of Co $L_{2,3}$ XAS.

**4.3. Co $L_{2,3}$ Edge.** The valence of the cobalt dopant in the manganese perovskites was investigated by Co $L_{2,3}$ XAS (Figure 4A). The spectrum of CoO single crystal was collected as the reference of $Co^{2+}$ in $O_h$ symmetry. A spectrum with almost the same features was reported by van Schooneveld et al.[30,31] In that work an octahedral structure for $Co^{2+}$ (HS) with a small tetragonal distortion (Ds = 0.02 eV) was suggested. By comparing the $L_{2,3}$ spectrum of $LaMn_{0.75}Co_{0.25}O_3$ (Figure 4d) with the CoO, reference compound of $Co^{2+}$, it can be concluded that the Co contained in this sample is octahedral $Co^{2+}$. The difference in the features between ∼778 and ∼782 eV is due to the presence of stronger covalency in the $LaMn_{0.75}Co_{0.25}O_3$ sample. Figure 4A shows that by Co doping the $L_{2,3}$ shifts toward higher energies and for $LaCoO_3$ the $L_3$ reaches to ∼781 eV. According to previous reports, this excitation energy is related to $Co^{3+}$.[13,32−34] The spectra indicate that the Co contained in the $LaMn_{0.5}Co_{0.5}O_3$ and $LaMn_{0.25}Co_{0.75}O_3$ samples is a mixture of $Co^{2+}$ and $Co^{3+}$. This confirms a $Mn^{3+} + Co^{3+} \rightarrow Mn^{4+} + Co^{2+}$ type of charge redistribution. The results clearly indicate that manganese enters to the $LaCoO_3$ as $Mn^{4+}$, while $Co^{2+}$ is doped into $LaMnO_3$.

Figure 4B shows the comparison of experimental Co $L_{2,3}$ XAS with multiplet calculations which were performed with the CTM4XAS interface.[16] The parameters used for the calculations are provided in Table 2. In the case of cobalt, we modeled covalency by the use of charge transfer parameters. The Slater−Condon parameters, used to describe the Coulomb repulsion and exchange interactions, are their atomic values which


DOI: 10.1021/acs.jpcc.6b00949
J. Phys. Chem. C 2016, 120, 8167−8174

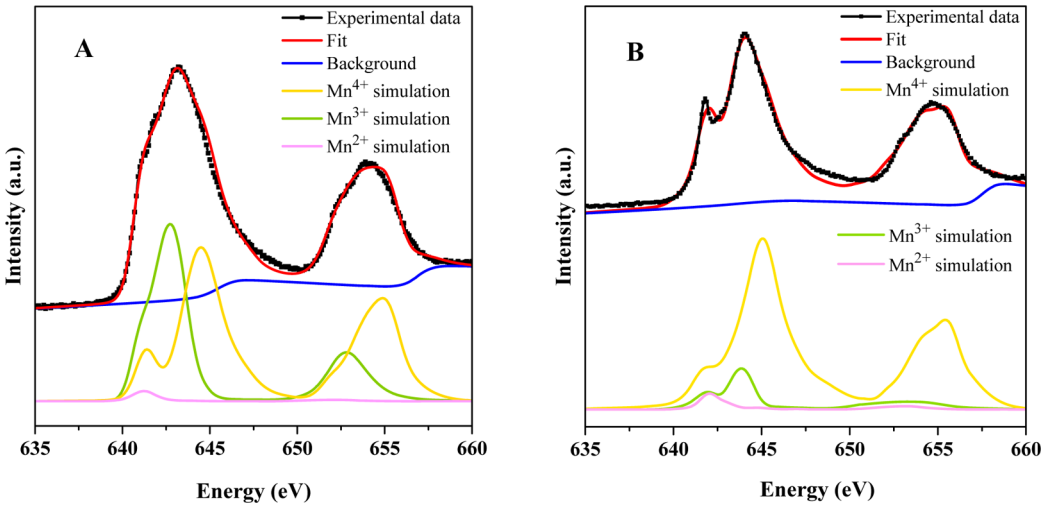


**Figure 3.** Multiplet calculation-based simulations of the experimental Mn L-edge data of $LaMnO_3$ (A) and $LaMn_{0.25}Co_{0.75}O_3$ (B). The bottom panel gives the simulations for the different Mn valences. The top panel compares the added simulated spectra with experiment. The obtained parameters are listed in Table 1.

**Table 1. Crystal Field, Charge Transfer, and Broadening Parameters Obtained from the Fitting of Multiplet Simulations to the Experimental Mn L-edge XAS Spectra of $LaMnO_3$ and $LaMn_{0.25}Co_{0.75}O_3$[a]**

| sample composition | site symmetry | ionic crystal field | Ds | Dt | Γ (fwhm) | G (fwhm) |
|---|---|---|---|---|---|---|
| $LaMnO_3$ | $Mn^{3+}$ ($D_{4h}$) | 1.53 | 0.06 | −0.01 | 0.1 ($L_3$)/ 2.0 ($L_2$) | 1.27 |
| | $Mn^{4+}$ ($O_h$) | 2.38 | – | – | 0.3 ($L_3$)/ 0.8 ($L_2$) | 1.27 |
| $LaMn_{0.25}Co_{0.75}O_3$ | $Mn^{4+}$ ($O_h$) | 2.34 | – | – | 0.4 ($L_3$)/ 1.2 ($L_2$) | 1.04 |

[a]All values are in eV.

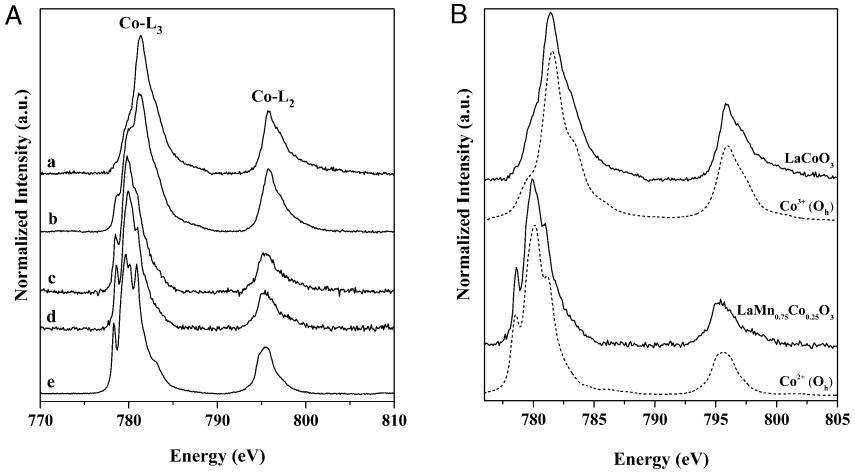


**Figure 4.** (A) Co 2p XAS spectra of (a) $LaCoO_3$, (b) $LaMn_{0.25}Co_{0.75}O_3$, (c) $LaMn_{0.5}Co_{0.5}O_3$, (d) $LaMn_{0.75}Co_{0.25}O_3$, and (e) CoO. (B) Co 2p XAS of $LaCoO_3$ and $LaMn_{0.75}Co_{0.25}O_3$ (solid lines) compared to crystal-field multiplet calculation (dots). The parameters used are listed in Table 2.

correspond to 80% of their Hartree−Fock values. The crystal field, 10 Dq, values reported in Table 2, correspond to its ionic contribution. Overall simulations confirm that $LaCoO_3$ mostly consists of octahedral $Co^{3+}$, and $LaMn_{0.75}Co_{0.25}O_3$ consists of octahedral $Co^{2+}$. The XRD results show that $LaCoO_3$ crystallizes in the rhombohedrally distorted cubic perovskite structure (Figure 1). The main structural motif of this material is a nearly perfect $CoO_6$ octahedron. The rhombohedral distortion of the cubic perovskite structure can be described by deformation along the body diagonal so that the angle of the Co−O−Co bond has changed from 180° to ∼163°.[35]

Considering charge transfer effects, the total amount of 10 Dq can be considered to be the sum of 10 $Dq_{ion}$ and 10 $Dq_{ct}$. The amount of 10 $Dq_{ct}$ for $Co^{2+}$ ($O_h$) and $Co^{3+}$ ($O_h$) is ∼0.4 and ∼0.5 eV, respectively, according to a series of simulations performed with increasing values of Δ (see Figure S1 in the Supporting Information). This assumption leads to the 10 $Dq_{total}$ of ∼1.1 for $Co^{2+}$ and ∼2.2 for $Co^{3+}$, which are in agreement with previous studies.[23,30,36]

### 4.4. The Ground-State Composition of $Mn^{3+}$ and $Co^{3+}$.

The parameters listed in Tables 1 and 2 were used for calculating the ground-state composition of $Mn^{3+}$ (in $LaMnO_3$) and $Co^{3+}$ (in $LaCoO_3$) by the CTM4DOC program (Table 3). It was reported that in $LaCoO_3$ and $LaMnO_3$ both $U_{dd}$ and Δ are of similar strengths, and thus these compounds cannot be classified as a purely charge transfer or a Mott Hubbard insulator, but have



DOI: 10.1021/acs.jpcc.6b00949
J. Phys. Chem. C 2016, 120, 8167−8174

**Table 2. Crystal Field, Charge Transfer, and Broadening Parameters Used for the Calculation of Theoretical Co L-Edge XAS Spectra of $LaCoO_3$ and $LaMn_{0.75}Co_{0.25}O_3$[a]**

| sample composition | site symmetry | ionic crystal field | charge transfer energy [Δ] | Γ (fwhm) | G (fwhm) |
|---|---|---|---|---|---|
| $LaCoO_3$[b] | $Co^{3+}$ ($O_h$) | 1.7 | 4.5 | 0.6 ($L_3$) 1.2 ($L_2$) | 0.25 |
| $LaMn_{0.75}Co_{0.25}O_3$[b] | $Co^{2+}$ ($O_h$) | 0.7 | 3 | 0.5 ($L_3$) 0.8 ($L_2$) | 0.15 |

[a]All values are in eV. [b]Hopping parameters for $e_g$ and $t_{2g}$ electrons are 2 and 1, respectively. Core hole potential $Q$ and the 3d3d repulsion energy $U$, are assumed to be 7 and 6 eV, respectively.

mixed character.[37] The nature of the ground states indicated that these oxides are highly mixed valent with a large hopping matrix element.

The results show that $LaCoO_3$ mostly consists of octahedral low-spin ($^1A_1$) $Co^{3+}$ with the admixture as given in Table 3. Abbate et al.[38] have mentioned that at low temperatures the low spin state of $LaCoO_3$ shows a shoulder located at 781.5 eV, i.e., at the higher energy region of the $L_3$-edge peak. They suggested that the absence of the shoulder at 781.5 eV and the increased intensity around 778 eV, i.e., the lower energy region of the $L_3$-edge peak, can be attributed to thermally populated high-spin state. Table 3 lists the obtained $Mn^{3+}$ ground state of $LaMnO_3$ in the $D_{4h}$ symmetry and then approximated as octahedral. These results imply that $Mn^{3+}$ is in a mixed-spin state with ∼80% low-spin ($S = 1$) and ∼20% high-spin ($S = 2$) character.

**4.5. Mn and Co $L_{2,3}$ Data Analysis Based on Experimental References.** To determine the valence composition of Mn and Co, the experimental data were analyzed using a holistic model that included the background and references for both metals to fit the experimental data using the methodology implemented in Blueprint XAS to obtain a family of good fits. The first step was the choice of reference compounds for specific valence of each transition metal. The analysis of Mn and Co L-edge shifts was performed using edge energies of $LaMnO_3$, $LaMn_{0.25}Co_{0.75}O_3$, $LaCoO_3$, and $LaMn_{0.75}Co_{0.25}O_3$ samples as references for formal valence states of $Mn^{3+}$, $Mn^{4+}$, $Co^{3+}$, and $Co^{2+}$, respectively. Figure 5 reflects the results from these fits. In case of Co $L_{2,3}$, the fits reproduce the experimental spectra adequately. For Mn, despite a good general agreement, the fits could not properly replicate the feature observed in the experimental data in the range of ∼640−642 eV. As shown in Figure 2, this range can be an indication of the presence of a small amount of $Mn^{2+}$ in the samples. To calculate the amount of $Mn^{4+}$ contained in $LaMnO_3$, the XAS spectrum of $LaMn_{0.25}Co_{0.75}O_3$, i.e., the reference of $Mn^{4+}$, was subtracted from $LaMnO_3$ in different proportions (see Figure S2 in the Supporting Information). Results showed that the average oxidation state of Mn in $LaMnO_3$ is +3.13, which is in good agreement with XRD results. The average valence states derived for $LaMn_{1-x}Co_xO_3$ series according to this data analysis are presented in Table 4.

**4.6. The Oxygen K-Edge.** Complementary information on the role of dopant in the bonding of these series of compounds can be obtained from the O K-edge (Figure 6). In general, the peaks at ∼530, 536, and 545 eV correspond to the excitation from an oxygen 1s orbital to hybridized O 2p-Mn/Co 3d, O 2p-La 5d, and O 2p-Mn/Co 4sp orbitals, respectively. A direct comparison of these experimental spectra shows important similarities in the number and shape of the different peaks between these compounds. The only difference is a small shift in the energy position of the second and third peaks. This similarity is expected as the second feature (∼536 eV) corresponds to the La 5d states, which is assumed to be identical for all of the samples. The third feature (∼545 eV) is attributed to transition metal 4sp state, which generally has a wider bandwidth and therefore is largely similar for Mn and Co. The position of the first peak of the oxygen K-edge does not seem to change position, which is not what is usually expected for mixed valence systems. In general, the edge position of the oxygen K-edge shows a number of different behaviors for different metals and different combinations of valences. In some cases there is a clear shift, for example for the equivalent Co, Ni, and Cu trivalent oxides ($La_2(Li,Cu)O_4$) and for nickel where the edge of $Ni^{3+}$ is shifted with respect to $Ni^{2+}$.[39] In the case of manganese and cobalt the situation is not so clear. A study of $La(Sr)MnO_3$ showed essentially no shift from $Mn^{3+}$ to $Mn^{4+}$.[40] This is probably because the difference between $Mn^{3+}$ and $Mn^{4+}$ is an extra hole in the $e_g$-state (for high-spin), but no new orbital comes available. In the case of cobalt, there is a clear shift in $La(Sr)CoO_3$, and $Co^{4+}$ has an energy lower than that of $Co^{3+}$.[41] This is due to the hole in the $t_{2g}$-state for the $3d^5$-system $Co^{4+}$. The same shift is visible for the $Li_{(1-x)}CoO_2$ system.[42] Looking at the mixed valent $Co^{2+}/Co^{3+}$ systems, there is no shift in the oxygen K-edge between CoO and $LiCoO_2$.

It turns out that the $Co^{2+}/Co^{3+}$ and also the $Mn^{3+}/Mn^{4+}$ oxides do not shift, and also the edge position of these systems is approximately 530 eV. This implies that we do not expect shifts in the oxygen K-edge, as all four constituting ions $Co^{2+}/Co^{3+}/Mn^{3+}/Mn^{4+}$ have oxygen K-edges at the same edge energy.

**Table 3. Ground-State Composition (%) of $Co^{3+}$ and $Mn^{3+}$ Ions in $LaCoO_3$ and $LaMnO_3$ Samples, Respectively[a]**

| | | | | | | |
|---|---|---|---|---|---|---|
| | | | $LaCoO_3$ | | | |
| Symmetry | $t_2^6e^0$ | $t_2^6e^1\underline{L}$ | $t_2^4e^2$ | $t_2^5e^1$ | $t_2^5e^2\underline{L}$ | $t_2^4e^3\underline{L}$ |
| $O_h$ | 68.2 | 19.8 | 6.0 | 3.9 | 1.0 | 0.9 |
| | | | $LaMnO_3$ | | | |
| $D_{4h}$ | $e^3b_2^1a_1^0b_1^0$ | $e^2b_2^1a_1^1b_1^0$ | $e^2b_2^2a_1^0b_1^0$ | $e^3b_2^0a_1^1b_1^0$ | $e^2b_2^1a_1^0b_1^1$ | $e^1b_2^1a_1^0b_1^2$ |
| | 83.9 | 11.5 | 1.5 | 0.7 | 0.6 | 0.6 |
| $O_h$ | $t_2^4e^0$ | $t_2^3e^1$ | $t_2^2e^2$ | | | |
| | 80.6 | 18.3 | 1.1 | | | |

[a]Results are obtained from projections in CTM4DOC using the parameters that fit the experimental Mn and Co L-edge XAS of $LaMnO_3$ and $LaCoO_3$ and that are listed in Table 1 and Table 2, respectively. The 3d orbitals are divided into $t_{2g}$ and $e_g$ orbitals in octahedral ($O_h$) symmetry and into $a_{1g}$ ($d_{z2}$), $b_{1g}$ ($d_{x2-y2}$), $b_{2g}$ ($d_{xy}$), and $e_g$ ($d_{xz}$,$d_{yz}$) orbitals in tetragonal ($D_{4h}$) symmetry. We omit the gerade ($g$) symbol to simplify the configurations. $\underline{L}$ defines a ligand hole.



DOI: 10.1021/acs.jpcc.6b00949
J. Phys. Chem. C 2016, 120, 8167−8174

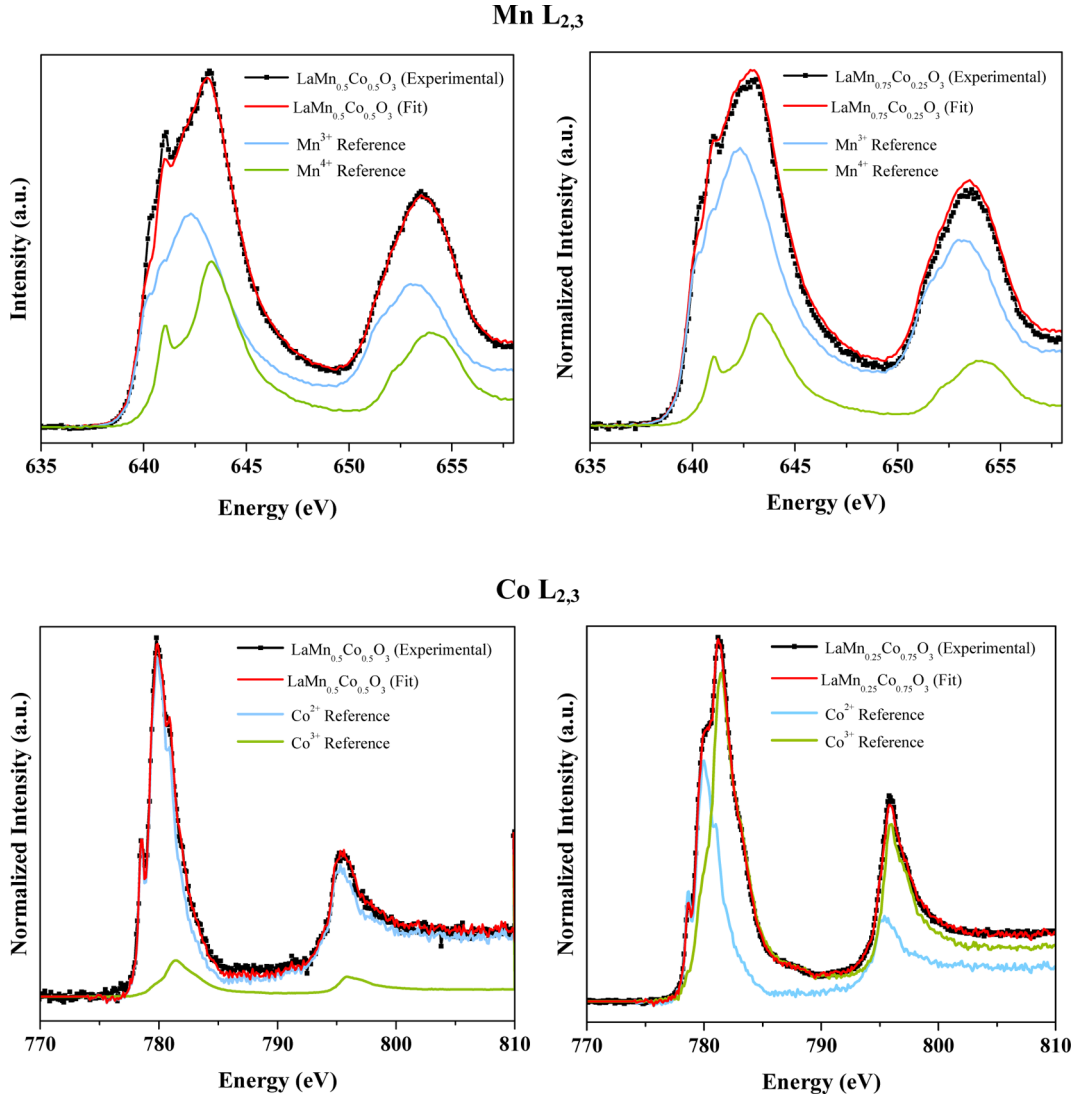


**Figure 5.** Representative fit to the experimental spectra for $LaMn_{0.25}Co_{0.75}O_3$, $LaMn_{0.5}Co_{0.5}O_3$, and $LaMn_{0.75}Co_{0.25}O_3$ samples. Here $LaMnO_3$, $LaMn_{0.25}Co_{0.75}O_3$, $LaCoO_3$, and $LaMn_{0.75}Co_{0.25}O_3$ experimental data are used as references for formal valence states: $Mn^{3+}$, $Mn^{4+}$, $Co^{3+}$, and $Co^{2+}$, respectively.

**Table 4. Contributions of Manganese and Cobalt Oxidation States Obtained from Figure 5**[a]

| no. | sample composition | $Mn^{3+}$ (%) | $Mn^{4+}$ (%) | $Co^{2+}$ (%) | $Co^{3+}$ (%) | std dev of Mn | std dev of Co | Mn valence | Co valence | TM valence |
|---|---|---|---|---|---|---|---|---|---|---|
| 1 | $LaMnO_3$ | 87 | 13 | – | – | – | – | 3.13 | – | +3.13 |
| 2 | $LaMn_{0.75}Co_{0.25}O_3$ | 68.5 | 31.5 | 100 | – | 6.33 | – | 3.32 | 2.00 | +2.99 |
| 3 | $LaMn_{0.5}Co_{0.5}O_3$ | 58.5 | 41.5 | 85.0 | 15.0 | 7.79 | 6.38 | 3.42 | 2.15 | +2.78 |
| 4 | $LaMn_{0.25}Co_{0.75}O_3$ | – | 100 | 33.9 | 66.1 | – | 5.75 | 4.00 | 2.66 | +3.00 |
| 5 | $LaCoO_3$ | – | – | – | 100 | – | – | – | 3.00 | +3.00 |

[a]"TM valence" is an *x*-weighted average of Co and Mn average oxidation states, which is supposed to be equal to 3.00 in the case of perfect oxygen stoichiometry. Std dev stands for standard deviation.

We employed the first peak of the O K-edge spectra to assess the extent of Mn/Co 3d-O 2p hybridization among the series. Table 5 shows the results from fitting of empirical pseudo-Voigt to account for the different bound transitions and of an empirical cumulative pseudo-Voigt to account for the rising edge to the experimental spectra by using Blueprint XAS. The intensity-area of the oxygen K pre-edge feature, which reflects the covalency, was normalized with respect to the total intensity of O 2p-La 5d peaks. These results are consistent with the notion that covalency coefficient increases with the nominal number of 3d electrons and with a previous report by Suntivich et al.[43]

## 5. CONCLUSIONS

A detailed investigation of the ground-state symmetry and the electronic structure of Mn and Co in $LaMn_{1-x}Co_xO_3$ series has been carried out using soft X-ray spectroscopy. Experimental O 1s, Mn 2p, and Co 2p XAS data were accompanied by theoretical calculations, using the CTM4XAS, CTM4DOC, and Blueprint XAS programs to probe the changes of Mn and Co electronic



DOI: 10.1021/acs.jpcc.6b00949
J. Phys. Chem. C 2016, 120, 8167−8174

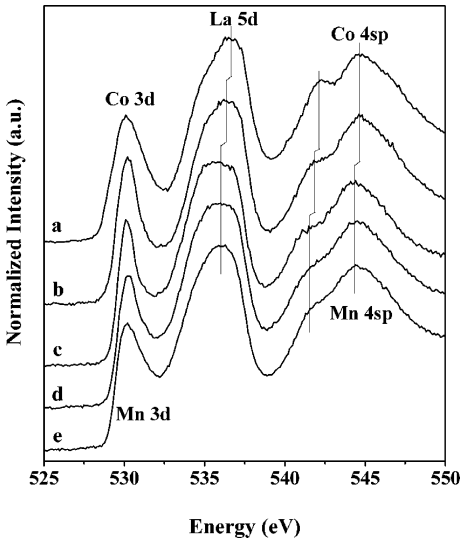


**Figure 6.** O 1s XAS spectra of (a) $LaCoO_3$, (b) $LaMn_{0.25}Co_{0.75}O_3$, (c) $LaMn_{0.5}Co_{0.5}O_3$, (d) $LaMn_{0.75}Co_{0.25}O_3$, and (e) $LaMnO_3$.

**Table 5. Calculated Covalency Coefficients of $LaMn_{1-x}Co_xO_3$ Samples**

| sample | normalized pre-edge intensity | standard deviation |
|---|---|---|
| $LaMnO_3$ | 0.260 | 0.013 |
| $LaMn_{0.75}Co_{0.25}O_3$ | 0.256 | 0.032 |
| $LaMn_{0.5}Co_{0.5}O_3$ | 0.265 | 0.014 |
| $LaMn_{0.25}Co_{0.75}O_3$ | 0.338 | 0.038 |
| $LaCoO_3$ | 0.328 | 0.031 |

structure due to doping. A detailed analysis of X-ray absorption data showed that by cobalt doping the oxidation state of Mn and Co increases. Due to the fact that covalency increases with the formal valence for a given transition metal, the development of the oxygen prepeak is a measure for the development of the oxidation state of the transition metal. Oxidation of the transition metal was found to increase hybridization, which may reflect the reduced transition metal 3d and oxygen 2p energy difference, causing increased covalency. The ground state of $Mn^{3+}$ and $Co^{3+}$ is determined to be mainly low-spin, with 10% to 20% quantum-chemical admixture of high-spin states into a mixed-spin ground state. In most previous studies $LaCoO_3$ was considered to be an ionic/ligand fieldlike system and the $Co^{3+}$ was reported to be in a low-spin state at room temperature. Transition of low-spin state $t_{2g}^6 e_g^0$ to intermediate-spin state $t_2g^5 e_g^1$ of $Co^{3+}$ ions takes place due to the competition of crystal-field $t_{2g}$-$e_g$ splitting and effective exchange interaction of 3d spin orbitals. The oxides, corresponding to high formal oxidation states, may be negative charge transfer systems. It results in an essential modification of the electronic structure, in particular in a possible stabilization of an intermediate state. Lastly, we confirm that the present study describes an efficient approach to systematically investigate the electronic structure of transition metals, which can also be applied for other correlated systems.

It can be concluded that the $LaMn_{1-x}Co_xO_3$ series maintains its average trivalent metal site by combining the $Mn^{3+}$/ $Mn^{4+}$ balance in combination with the $Co^{2+}/Co^{3+}$ balance. In addition to the catalytic properties of the system, this also creates a tool to generate a system with the desired magnetic properties that are a fine balance between the different valences for Mn and Co in combination with their spin state that turns out to be exactly at the high-spin low-spin transition point.

## ■ ASSOCIATED CONTENT

### Supporting Information

The Supporting Information is available free of charge on the ACS Publications website at DOI: 10.1021/acs.jpcc.6b00949.

S1. The relation between the average 10 $Dq_{ct}$ and $\Delta$ for $Co^{2+}$ and $Co^{3+}$. The energy difference between ground state and first excitation state was converted to 10 $Dq_{total}$ according to the Tanabe−Sugano diagram. The 10 $Dq_{ct}$ was obtained from the subtraction of the 10 $Dq_{ionic}$ from the 10 $Dq_{total}$. The 10 $Dq_{ionic}$ is the value used in the CTM interface. S2. Subtracting the Mn 2p spectrum of $LaMn_{0.25}Co_{0.75}O_3$, $S_2$, from $LaMnO_3$, $S_1$, in different proportions (PDF)

## ■ AUTHOR INFORMATION

### Corresponding Authors

*E-mail: M.GhiasiKabiri@uu.nl. Tel: (+31) 302537400.
*E-mail: F.M.F.deGroot@uu.nl. Tel: (+31) 302537400.

### Notes

The authors declare no competing financial interest.

## ■ ACKNOWLEDGMENTS

We thank H.Z.B. for the allocation of synchrotron radiation beamtime at the UE52-SGM beamline of the BESSY II synchrotron. This work was financially supported by an ERC advanced grant XRAYonACTIVE, number 340279.

## ■ REFERENCES

(1) Singh, S. J.; Jayaram, R. V. Oxidation of Alkylaromatics to Benzylic Ketones Using TBHP as an Oxidant over $LaMO_3$ (M = Cr Co, Fe, Mn, Ni) Perovskites. *Catal. Commun.* **2009**, *10*, 2004−2007.

(2) Daengsakul, S.; Thomas, C.; Thomas, I.; Mongkolkachit, C.; Siri, S.; Amornkitbamrung, V.; Maensiri, S. Magnetic and Cytotoxicity Properties of $La_{1-x}Sr_xMnO_3$ ($0 \le x \le 0.5$) Nanoparticles Prepared by a Simple Thermal Hydro-decomposition. *Nanoscale Res. Lett.* **2009**, *4*, 839−845.

(3) Ghiasi, M.; Malekzadeh, A. Solar Photocatalytic Degradation of Methyl Orange over $La_{0.7}Sr_{0.3}MnO_3$ Nano-perovskite. *Sep. Purif. Technol.* **2014**, *134*, 12−19.

(4) Haghiri-Gosnet, A. M.; Renard, J. P. CMR Manganites: Physics, Thin Films and Devices. *J. Phys. D: Appl. Phys.* **2003**, *36*, 127−150.

(5) Autret, C.; Hejtmanek, J.; Knizek, K.; Marysko, M.; Jirak, Z.; Dlouha, M.; Vratislav, S. Electric Transport and Magnetic Properties of Perovskites $LaMn_{1-x}Co_xO_3$ up to 900K. *J. Phys.: Condens. Matter* **2005**, *17*, 1601−1616.

(6) Dezanneau, G.; Audier, M.; Vincent, H.; Meneghini, C.; Djurado, E. Structural Characterization of $La_{1-x}MnO_{3\pm\delta}$ by X-ray Diffraction and X-ray Absorption Spectroscopy. *Phys. Rev. B: Condens. Matter Mater. Phys.* **2004**, *69*, 014412.

(7) Barilo, S. N.; Gatalskaya, V. I.; Shiryaev, S. V.; Kurochkin, L. A.; Ustinovich, S. N.; Szymczak, H.; Szymczak, R.; Baran, M. Magnetic Behavior of Single Crystals of the Perovskite Oxides $LaMn_{1-x}Co_xO_3$. *Phys. Status Solidi A* **2003**, *199* (3), 484−490.

(8) Goodenough, J. B.; Wold, A.; Arnott, R. J.; Menyuk, N. Relationship Between Crystal Symmetry and Magnetic Properties of Ionic Compounds Containing $Mn^{3+}$. *Phys. Rev.* **1961**, *124*, 373−384.

(9) Park, J. H.; Cheong, S. W.; Chen, C. T. Double-exchange Ferromagnetism in $La(Mn_{1-x}Co_x)O_3$. *Phys. Rev. B: Condens. Matter Mater. Phys.* **1997**, *55*, 11072−11075.

(10) Troyanchuk, I. O.; Lobanovsky, L. S.; Khalyavin, D. D.; Pastushonok, S. N.; Szymczak, H. Magnetic and Magnetotransport



DOI: 10.1021/acs.jpcc.6b00949
J. Phys. Chem. C 2016, 120, 8167−8174

Properties of Co-doped Manganites with Perovskite Structure. *J. Magn. Magn. Mater.* **2000**, *210*, 63−72.
(11) Sikora, M.; Kapusta, C.; Knížek, K.; Jirák, Z.; Autret, C.; Borowiec, M.; Oates, C. J.; Procházka, V.; Rybicki, D.; Zajac, D. X-ray Absorption Near-edge Spectroscopy Study of Mn and Co Valence States in $LaMn_{1-x}Co_xO_3$ (x = 0−1). *Phys. Rev. B: Condens. Matter Mater. Phys.* **2006**, *73*, 094426.
(12) Sikora, M.; Knizek, K.; Kapusta, Cz.; Glatzel, P. Evolution of Charge and Spin State of Transition Metals in the $LaMn_{1-x}Co_xO_3$ Perovskite Series. *J. Appl. Phys.* **2008**, *103*, 07C907.
(13) Burnus, T.; Hu, Z.; Hsieh, H. H.; Joly, V. L. J.; Joy, P. A.; Haverkort, M. W.; Wu, H.; Tanaka, A.; Lin, H. J.; Chen, C. T.; Tjeng, L. H. Local Electronic Structure and Magnetic Properties of $LaMn_{0.5}Co_{0.5}O_3$ Studied by X-ray Absorption and Magnetic Circular Dichroism Spectroscopy. *Phys. Rev. B: Condens. Matter Mater. Phys.* **2008**, *77*, 125124.
(14) Palikundwar, U. A.; Sapre, V. B.; Moharil, S. V.; Priolkar, K. R. Local Structure Around Mn and Co in $LaMn_{1-x}Co_xO_{3\pm\delta}$: an EXAFS Study. *J. Phys.: Condens. Matter* **2009**, *21*, 235405.
(15) Frozandeh-Mehr, E.; Malekzadeh, A.; Ghiasi, M.; Gholizadeh, A.; Mortazavi, Y.; Khodadadi, A. Effect of Partial Substitution of Lanthanum by Strontium or Bismuth on Structural Features of the Lanthanum Manganite Nanoparticles as a Catalyst for Carbon Monoxide Oxidation. *Catal. Commun.* **2012**, *28*, 32−37.
(16) Stavitski, E.; de Groot, F. M. F. The CTM4XAS Program for EELS and XAS Spectral Shape Analysis of Transition Metal L Edges. *Micron* **2010**, *41*, 687−694.
(17) Thole, B. T.; van der Laan, G.; Fuggle, J. C.; Sawatzky, G. A.; Karnatak, R. C.; Esteva, J. M. 3d X-ray-absorption Lines and the $3d^9 4f^{n+1}$Multiplets of the Lanthanides. *Phys. Rev. B: Condens. Matter Mater. Phys.* **1985**, *32*, 5107−5118.
(18) Cowan, R. D. *The Theory of Atomic Structure and Spectra*; University of California Press: Berkeley, 1981.
(19) Butler, P. H. *Point Group Symmetry Applications: Methods and Tables*; Plenum Press: New York, 1981.
(20) de Groot, F.; Kotani, A. Core Level Spectroscopy of Solids. *Advances in Condensed Matter Science*; CRC: Boca Raton, FL, 2008.
(21) Delgado-Jaime, M. U.; Mewis, C. P.; Kennepohl, P. Blueprint XAS: a Matlab-based Toolbox for the Fitting and Analysis of XAS Spectra. *J. Synchrotron Radiat.* **2010**, *17*, 132−137.
(22) Delgado-Jaime, M. U.; Kennepohl, P. Development and Exploration of a New Methodology for the Fitting and Analysis of XAS Data. *J. Synchrotron Radiat.* **2010**, *17*, 119−128.
(23) Wasinger, E. C.; de Groot, F. M. F.; Hedman, B.; Hodgson, K. O.; Solomon, E. I. L-edge X-ray Absorption Spectroscopy of Non-Heme Iron Sites: Experimental Determination of Differential Orbital Covalency. *J. Am. Chem. Soc.* **2003**, *125*, 12894−12906.
(24) Yang, Z.; Ye, L.; Xie, X. Electronic and Magnetic Properties of the Perovskite Oxides: $LaMn_{1-x}Co_xO_3$. *Phys. Rev. B: Condens. Matter Mater. Phys.* **1999**, *59*, 7051−7057.
(25) Chen, X.; Cai, Q.; Wang, W.; Chen, Z.; Wu, Z.; Wu, Z. X-ray Diffraction and X-ray Absorption Spectroscopy Studies on the Chemical Transformation and Formation of Nanoscale $LaMnO_{3.12}$. *J. Phys. Chem. C* **2007**, *111*, 4512−4518.
(26) Ghiasi, M.; Malekzadeh, A. Synthesis, Characterization and Photocatalytic Properties of Lanthanum Oxy-carbonate, Lanthanum Oxide and Lanthanum Hydroxide Nanoparticles. *Superlattices Microstruct.* **2015**, *77*, 295−304.
(27) Cramer, S. P.; de Groot, F. M. F.; Ma, Y.; Chen, C. T.; Sette, F.; Kipke, C. A.; Eichhorn, D. M.; Chan, M. K.; Armstrong, W. H.; Libby, E.; et al. Ligand Field Strengths and Oxidation States from Manganese L-Edge Spectroscopy. *J. Am. Chem. Soc.* **1991**, *113*, 7937−7940.
(28) de Groot, F. M. F. X-ray Absorption and Dichroism of Transition Metals and Their Compounds. *J. Electron Spectrosc. Relat. Phenom.* **1994**, *61*, 529−622.
(29) Radtke, G.; Maunders, C.; Lazar, S.; de Groot, F. M. F.; Etheridge, J.; Botton, G. A. The Role of Mn in the Electronic Structure of $Ba_3Ti_2MnO_9$. *J. Solid State Chem.* **2005**, *178*, 3426−3430.
(30) van Schooneveld, M. M.; Kurian, R.; Juhin, A.; Zhou, K.; Schlappa, J.; Strocov, V. N.; Schmitt, T.; de Groot, F. M. F. Electronic Structure of CoO Nanocrystals and a Single Crystal Probed by Resonant X-ray Emission Spectroscopy. *J. Phys. Chem. C* **2012**, *116*, 15218−15230.
(31) van Schooneveld, M. M.; Suljoti, E.; Campos-Cuerva, C.; Gosselink, R. W.; van der Eerden, A.; Schlappa, j.; Zhou, K.; Monney, C.; Schmitt, T.; de Groot, F. M. F. Transition Metal Nanoparticle Oxidation in a Chemically Non-homogenous Environment Revealed by 2p3d Resonant X-ray Emission. *J. Phys. Chem. Lett.* **2013**, *4*, 1161−1166.
(32) Morales, F.; de Groot, F. M. F.; Glatzel, P.; Kleimenov, E.; Bluhm, H.; Havecker, M.; Knop-Gericke, A.; Weckhuysen, B. M. In Situ X-ray Absorption of $Co/Mn/TiO_2$ Catalysts for Fischer−Tropsch Synthesis. *J. Phys. Chem. B* **2004**, *108*, 16201−16207.
(33) van Elp, J.; Wieland, J. L.; Eskes, H.; Kuiper, P.; Sawatzky, G. A.; de Groot, F. M. F.; Turner, T. S. Electronic Structure of CoO, Li-doped CoO, and $LiCoO_2$. *Phys. Rev. B: Condens. Matter Mater. Phys.* **1991**, *44*, 6090−6103.
(34) Orikasa, Y.; Ina, T.; Nakao, T.; Mineshige, A.; Amezawa, K.; Oishi, M.; Arai, H.; Ogumi, Z.; Uchimoto, Y. X-ray Absorption Spectroscopic Study on $La_{0.6}Sr_{0.4}CoO_{3-\delta}$ Cathode Materials Related with Oxygen Vacancy Formation. *J. Phys. Chem. C* **2011**, *115*, 16433−16438.
(35) Nekrasov, I. A.; Streltsov, S. V.; Korotin, M. A.; Anisimov, V. I. Influence of Rare-earth Ion Radii on the Low-spin to Intermediate-spin State Transition in Lanthanide Cobaltite Perovskites: $LaCoO_3$ Versus $HoCoO_3$. *Phys. Rev. B: Condens. Matter Mater. Phys.* **2003**, *68*, 235113.
(36) Haverkort, M. W.; Hu, Z.; Cezar, J. C.; Burnus, T.; Hartmann, H.; Reuther, M.; Zobel, C.; Lorenz, T.; Tanaka, A.; Brookes, N. B.; et al. Spin State Transition in $LaCoO_3$ Studied Using Soft X-ray Absorption Spectroscopy and Magnetic Circular Dichroism. *Phys. Rev. Lett.* **2006**, *97*, 176405.
(37) Barman, S. R.; Sarma, D. D. Photoelectron-spectroscopy Investigation of the Spin-state Transition in $LaCoO_3$. *Phys. Rev. B: Condens. Matter Mater. Phys.* **1994**, *49*, 13979.
(38) Abbate, M.; Fuggle, J. C.; Fujimori, A.; Tjeng, L. H.; Chen, C. T.; Potze, R.; Sawatzky, G. A.; Eisaki, H.; Uchida, S. Electronic Structure and Spin-state Transition of $LaCoO_3$. *Phys. Rev. B: Condens. Matter Mater. Phys.* **1993**, *47*, 16124.
(39) Hu, A.; Mazumdar, C.; Kaindl, G.; de Groot, F. M. F.; Warda, S. A.; Reinen, D. Valence Electron Distribution in $La_2Li_{1/2}Cu_{1/2}O_4$, $Nd_2Li_{1/2}Ni_{1/2}O_4$, and $La_2Li_{1/2}Co_{1/2}O_4$. *Chem. Phys. Lett.* **1998**, *297*, 321−328.
(40) Abbate, M.; de Groot, F. M. F.; Fuggle, J. C.; Fujimori, A.; Strebel, O.; Lopez, F.; Domke, M.; Kaindl, G.; Thole, B. T.; Sawatzky, G. A.; et al. Controlled-valence Properties of $La_{1-x}Sr_xFeO_3$ and $La_{1-x}Sr_xMnO_3$ Studied by Soft-x-ray Absorption Spectroscopy. *Phys. Rev. B: Condens. Matter Mater. Phys.* **1992**, *46*, 4511−4519.
(41) Hu, Z.; Grazioli, C.; Knupfer, M.; Golden, M. S.; Fink, J.; Mahadevan, P.; Kumar, A.; Ray, S.; Sarma, D. D.; Warda, S. A.; et al. Difference in Spin State and Covalence between $La_{1-x}Sr_xCoO_3$ and $La_{2-x}Sr_xLi_{0.5}Co_{0.5}O_4$. *J. Alloys Compd.* **2002**, *343*, 5−13.
(42) Yoon, W.-S.; Kim, K.-B.; Kim, M.-G.; Lee, M.-K.; Shin, H.-J.; Lee, J.-M.; Lee, J.-S. Oxygen Contribution on Li-Ion Intercalation-Deintercalation in $LiCoO_2$ Investigated by O K-Edge and Co L-Edge X-ray Absorption Spectroscopy. *J. Phys. Chem. B* **2002**, *106*, 2526−2532.
(43) Suntivich, J.; Hong, W. T.; Lee, Y.; Rondinelli, J. M.; Yang, W.; Goodenough, J. B.; Dabrowski, B.; Freeland, J. W.; Shao-Horn, Y. Estimating Hybridization of Transition Metal and Oxygen States in Perovskites from O K-edge X-ray Absorption Spectroscopy. *J. Phys. Chem. C* **2014**, *118*, 1856−1863.


DOI: 10.1021/acs.jpcc.6b00949
*J. Phys. Chem. C* 2016, 120, 8167−8174